Reduced Kinetic Mechanisms for Modelling LPP Combustion in Gas Turbines

A. Liñán, M. Bollig
Universidad Politecnica de Madrid
Pza. Cardenal Cisneros 3, 28040 Madrid, Spain.

A. L. Sánchez
Universidad Carlos III
Butarque 15, 28911 Leganés, Spain.

B. Lázaro
SENER
Severo Ochoa 4, 28760 Tres Cantos, Spain.

1. SUMMARY

Lean premixed methane-air flames are investigated in an effort to facilitate the numerical description of CO and NO emissions in LPP (lean premixed prevaporized) combustion systems. Starting with a detailed chemistry description that includes 195 elementary steps, sensitivity procedures and steady-state approximations are introduced to obtain two different four-step reduced mechanisms, which employ either H or OH as the intermediate representing the radical-pool evolution. The resulting reduced mechanisms are especially well suited to describe high-pressure, lean premixed combustion. Based on the resulting flame structures, and following previous analyses, the mechanism is further simplified to give a two-step description, in which fuel is consumed and CO is produced according to the fast overall step $CH_4+3/2\ O_2 \rightarrow CO+2H_2O$, while CO is slowly oxidized according to the overall step $CO+1/2O_2 \rightarrow CO_2$. Because of its associated fast rate, fuel consumption takes place in thin layers, while CO oxidation occurs downstream in a distributed manner, in a region where CO is the only intermediate not in steady state. In this two-step description, the rate of fuel consumption is assigned a heuristic Arrhenius dependence that adequately reproduces laminar burning velocities, whereas the rate of CO oxidation is extracted from a reduced chemistry analysis. Preliminary results corresponding to one-dimensional unstrained flames indicate that the formulation reproduces well flame structures, including profiles of CO, temperature and radicals. The accuracy of the resulting profiles suggests that the proposed formulation can also be used to calculate NO emissions by appending the appropriate chemistry. Although methane is employed in the present study as a model fuel, the universal structure of the resulting CO oxidation region, independent of the fuel considered, enables the proposed formulation to be readily extended to other hydrocarbons.

2. REDUCED CHEMICAL KINETIC MECHANISMS

Four different test cases were selected for the present study. These test cases, which are shown in Table 1, are taken from the flight envelope definition of the E-engine cycle, the virtual gas turbine selected as representative during the EU research program LOWNOX-III.

As a preliminary step, a detailed chemical mechanism for methane oxidation was identified. The starting scheme contains 195 elementary reactions and 34 species, with elementary rates largely taken from recent recommendations of the CEC [1]. This detailed mechanism contains in particular the C_2 chain of fuel oxidation. Extensive calculations with this chemistry set incorporated for the chemistry description were performed for the test cases outlined in Table 1. Both unstrained and strained flames were considered.

Previous analyses have shown that in these lean environments the C_1 chain of methane oxidation suffices to model flame structures [2]. Also, the contribution of the prompt mechanism to the NOx production is unimportant in high-pressure, lean premixed flames. As a result, the C_2 chain can be neglected when describing the combustion process in LPP combustion chambers.

Test-Case	p (Bar)	Φ	T_u (K)	Description
A	18	0.6	800	Cruise
B	40	0.6	900	Take-off
C	8.5	0.45	600	Approach
D	16	0.5	700	Descent

Table 1.- LOWNOX-III LPP combustor operating envelope. The columns correspond to the chamber pressure, and to the equivalence ratio and temperature of the fresh mixture.

Through reaction flux and sensitivity analyses a short mechanism with 57 elementary reactions and 17 species was identified. Further simplification was achieved by introducing steady state approximations for intermediates, providing two different four-step reduced kinetic schemes.

The first reduced description, with CO, H_2, and H as intermediates not in steady state [2], results in the following four global reactions:

$$CH_4 + H_2O + 2H \Leftrightarrow 4H_2 + CO \qquad (I')$$

$$O_2 + 3H_2 \Leftrightarrow 2H + 2H_2O \qquad (II')$$

$$2H + M \Leftrightarrow H_2 + M \qquad (III')$$

$$CO + H_2O \Leftrightarrow CO_2 + H_2 \qquad (IV')$$

The second reduced description replaces H by OH, an alternative motivated by the relatively large OH concentrations observed in the computations, yielding the four overall reactions given below:

Paper presented at the RTO AVT Symposium on "Gas Turbine Engine Combustion, Emissions and Alternative Fuels", held in Lisbon, Portugal, 12-16 October 1998, and published in RTO MP-14.

$$CH_4 + 2OH \Leftrightarrow CO + H_2O + 2H_2 \quad (I'')$$
$$H_2 + O_2 \Leftrightarrow 2OH \quad (II'')$$
$$2OH + H_2 \Leftrightarrow 2H_2O \quad (III'')$$
$$CO + H_2O \Leftrightarrow CO_2 + H_2 \quad (IV'')$$

The above global steps represent the main chemical processes that occur during fuel oxidation. Thus, fuel consumption occurs according to the first step in a process that involves radical removal. The second step summarizes the hydrogen-oxygen chain branching reactions. The third reaction represents radical recombination, and the last step is the water-gas shift that converts the CO produced by the first step to CO_2.

A)

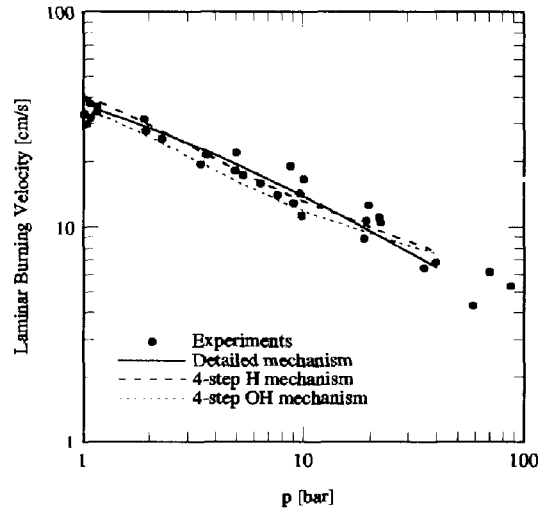

B)

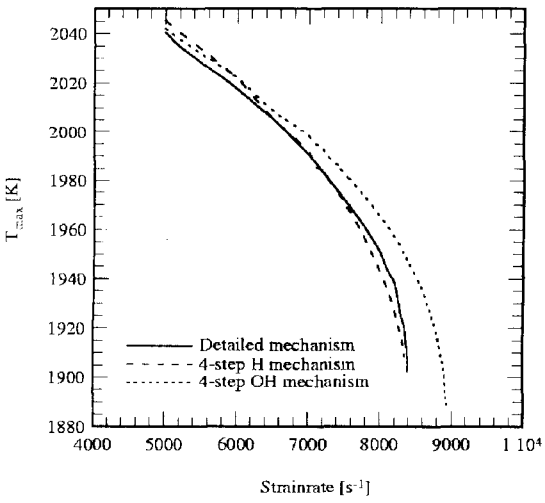

Figure 1: Laminar flame characteristics predicted by the two 4-step reduced schemes. A) Pressure dependence of the burning velocity for stoichiometric flames at T_u=298 K. B) Peak flame temperature under strained flow conditions (Test case A fresh mixture flowing against products at 1500 K)

The rates of the above global reactions depend on the rates of several elementary steps that compose the detailed chemistry set. In particular, it was found that incorporating methyl attack by HO_2 and OH is critical to obtain accurate results at elevated pressures, a characteristic not seen in previous studies [2].

As can be seen in Figure 1, both reduced chemistry descriptions give excellent results. In particular, the resulting laminar burning velocities, flame structures and radical concentration levels are found to be very accurate. In addition, strain effects are adequately captured, with the H-atom based reduced mechanism giving somewhat better predictions for the strain rate at extinction..

Since both mechanisms are analogous and give similar results, further analysis can be based on either reduced description. In what follows we select reactions I' to IV' for further developments, and retain only the main contributor to each of the overall reactions, thereby giving global rates (moles per unit volume per unit time) of the form:

$$\begin{aligned}\omega_{I'} &= k_{1f}[CH_4][H],\\ \omega_{II'} &= k_{2f}[O_2][H] - k_{2b}[O][OH],\\ \omega_{III'} &= k_{3f}[M][O_2][H] - k_{3b}[M][HO_2],\\ \omega_{IV'} &= k_{4f}[CO][OH] - k_{4b}[CO_2][H],\end{aligned} \quad (1)$$

where [i] denotes the concentration of chemical species i, M representing a third body, and k_{jf} and k_{jb} are the specific reaction-rate constants in the forward and backward directions for the elementary reactions:

$$CH_4 + H \overset{1}{\Rightarrow} CH_3 + H_2,$$
$$O_2 + H \overset{2}{\Leftrightarrow} O + OH,$$
$$O_2 + H + M \overset{3}{\Leftrightarrow} HO_2 + M,$$
$$CO + OH \overset{4}{\Leftrightarrow} CO_2 + H.$$

As explained below, if the reverse rate of reaction 3 were not included in the mechanism, then the resulting equilibrium concentrations of all intermediates would be zero, thereby potentially introducing significant errors in predictions of CO and NO formation. We therefore choose to retain this rate for increased accuracy.

Expressions for the different reaction-rate constants, with a third body efficiency equal to 0.4 introduced in computing [M], are given below in cm^3/mole/sec:

$$\begin{aligned}k_{1f} &= 1.300\cdot 10^4 T^{3.00}\exp(-4041/T),\\ k_{2f} &= 9.756\cdot 10^{13}\exp(-7469/T),\\ k_{2b} &= 1.445\cdot 10^{13}\exp(-352/T),\\ k_{3f}[M] &= 1.82\cdot 10^{16} T^{-1.80} p,\\ k_{3b} &= 5.058\cdot 10^{18} T^{0.80}\exp(-23574/T),\\ k_{4f} &= 4.400\cdot 10^6 T^{1.50}\exp(373/T),\\ k_{4b} &= 1.270\cdot 10^9 T^{1.50}\exp(-11872/T),\end{aligned}$$

where T and p are expressed in kelvins and atmospheres, respectively. Suitable simplified steady-state expressions for the concentrations of OH and O, necessary in evaluating Eq. 1 can be obtained by assuming partial equilibrium of reactions:

$$H_2 + OH \overset{5}{\Leftrightarrow} H_2O + H,$$
$$OH + OH \overset{6}{\Leftrightarrow} H_2O + O,$$

to give:

$$[OH] = K_5^{-1}[H_2O][H]/[H_2], \quad (2)$$

$$[O] = K_5^{-2}K_6[H_2O][H]^2/[H_2]^2, \quad (3)$$

Where K_5=0.227exp(7614/T) and K_6=0.0966exp(8573/T) are equilibrium constants. Similarly, the concentration of hydroperoxyl radicals needed to evaluate the backward rate of III' can be obtained from the truncated steady state expression:

$$[HO_2] = \frac{k_{3f}[M][O_2][H] + k_{7b}[O_2][H_2O]}{k_{3b}[M] + k_{7f}[OH]}, \quad (4)$$

Where the rate constants $k_{7f}=2.891\cdot10^{13}\exp(253/T)$ and $k_{7b}=3.069\cdot10^{14}\exp(-36083/T)$ (cm^3/mole/sec) correspond to the reaction:

$$HO_2 + OH \overset{7}{\Leftrightarrow} H_2O + O_2.$$

3. THE LIMIT OF SLOW CO OXIDATION

CO-oxidation is the slowest of the four chemical processes represented by I'-IV' [3]. To illustrate this, one can use Eq. 1 to give the characteristic chemical-time ratios $t_{I'}/t_{IV'}=k_{4f}/(k_{1f}K_5)$, $t_{II'}/t_{IV'}=k_{4f}/(k_{2f}K_5)$ and $t_{III'}/t_{IV'}=k_{4f}/(k3f[M]K_5)$. Evaluating the above estimates at the temperatures and pressures typical of gas turbine combustion yields the scaling law $t_{I'}\sim t_{II'}\sim t_{III'}\ll t_{IV'}$ (for instance, at T=1700 K and p= 30 atm, $t_{I'}/t_{IV'}=0.01$, $t_{II'}/t_{IV'}=0.016$, and $t_{III'}/t_{IV'}=0.022$). This scaling suggests that fuel consumption followed by radical branching and radical recombination occur in thin layers that exhibit small concentration of H_2 and radicals. CO oxidation is much slower, and consequently occurs in a distributed manner in a downstream region where in the first approximation $[CH_4]=0$ and H_2 and H maintain steady state [3]. Note in particular that fast radical removal through reaction I' causes all chemical activity to be frozen in the preheat zone upstream from the fuel-consumption layer [2].

The overall step describing the thin fuel-consumption layer can be obtained by eliminating H_2 and H by linear combination of I'-III' to give:

$$CH_4 + \frac{3}{2}O_2 \rightarrow CO + 2H_2O. \quad (I)$$

On the other hand, incorporating the steady states of H_2 and H into step IV' by linear combination with steps II' and III' provides the global CO-oxidation step:

$$CO + \frac{1}{2}O_2 \rightarrow CO_2. \quad (II)$$

The rate of reaction I, which is fundamental to determine the propagation velocity of the flame, is only extractable in terms of the rates of reactions I', II', and III' from a detailed study of the inner structure of the fuel-consumption layer, where both H and H_2 do not follow the steady-state approximation. Instead of further pursuing such an analysis, we choose to represent this rate by an Arrhenius law of the form

$$\omega_I = B[CH_4]\exp\left(-\frac{E}{R^oT}\right), \quad (5)$$

where R^o is the universal gas constant. The values of the activation energy E, and of the prexponential factor, B, must be chosen to adequately reproduce the steady flame propagation velocity. On the other hand, the rate of reaction II is given by:

$$\omega_{II} = \omega_{IV'} = k_{4f}[CO][OH] - k_{4b}[CO_2][H]. \quad (6)$$

As shown below, with appropriate choices for E and B to reproduce the flame propagation velocity, the CO oxidation rate given in Eq. 6 describes accurately the nonequilibrium evolution of the CO concentration, as well as its associated radical pool (through appropriate steady-state expressions), downstream from the fuel-consumption layer. Failure of the proposed two-step model within the thin fuel-consumption layer has only a limited effect as shown below.

In the CO-oxidation region, the corresponding steady-state equations for H_2 and H with $[CH_4]=0$, $-3\omega_{II'}+\omega_{III'}+\omega_{IV'}=0$ and $2\omega_{II'}-2\omega_{III'}=0$, can be solved to give the expression:

$$[H_2] = K_5^{-1}[O_2]^{-1}\alpha_1\{(K_6/K_2)[OH]^2 + \frac{1}{2}\left(\frac{k_{4f}}{k_{2f}}\right)[CO][H_2O]\}, \quad (7)$$

together with the fourth-order polynomial:

$$a_4[OH]^4 + a_3[OH]^3 + a_2[OH]^2 + a_1[OH] + a_0 = 0, \quad (8)$$

where we have introduced the coefficients:

$$\begin{aligned} a_4 &= -(K_6k_{7f}/K_2)[1-\alpha_1(1-\gamma)], \\ a_3 &= -(K_6k_{3b}/K_2)[1-\alpha_1][M], \\ a_2 &= \frac{1}{2}\alpha_1(k_{4f}k_{7f}/k_{2f})(1-\gamma)[CO][H_2O], \\ a_1 &= \frac{1}{2}\alpha_1(k_{4f}k_{3b}/k_{2f})[M][CO][H_2O], \\ a_0 &= \frac{1}{2}\alpha_1(k_{3b}k_{7b}/k_{2f})[M][H_2O]^2[O_2], \end{aligned} \quad (10)$$

and the functions

$$\alpha_1 = \left(1 + \frac{1}{2}\frac{k_{4f}}{k_{2f}}\frac{[CO_2]}{[O_2]}\right)^{-1} \quad (10)$$

and

$$\gamma = k_{3f}[M]/k_{2f} \quad (11)$$

Once Eq. 8 is solved for [OH], one can use Eq. 7 to compute $[H_2]$ and Eqs. 2 and 3 to calculate [H] and [O].

Note that, if the reverse of reaction III' is neglected in the formulation for simplicity, then Eqs. 7 and 8 reduce to the explicit expressions

$$[H_2] = \frac{1}{2}\frac{k_{4f}\alpha_2}{k_{3f}[M]K_5}\frac{[H_2O][CO]}{[O_2]} \quad (12)$$

and

$$[OH] = \left(\frac{1}{2} \frac{k_{4f} K_2 (1-\gamma)\alpha_2}{k_{3f}[M] K_6} \right)^{1/2} [H_2O]^{1/2} [CO]^{1/2} \quad (13)$$

where

$$\alpha_2 = \left(1 + \frac{1}{2} \frac{k_{4b}}{k_{3f}[M]} \frac{[CO_2]}{[O_2]} \right)^{-1} \quad (14)$$

Substituting then Eqs. 2, 12 and 13 into 6 yields

$$\omega_{II} = \left(\frac{k_{4f}^3 K_2 (1-\gamma)\alpha_2^3}{2 k_{3f}[M] K_6} \right)^{1/2} [H_2O]^{1/2} [CO]^{3/2} \quad (15)$$

as a simplified expression for the CO-oxidation rate corresponding to the limit of irreversible radical recombination.

4. CONSERVATION EQUATIONS

The conservation equations for the reactive species corresponding to the reproduced chemistry description I-II can be written as

$$\rho \frac{D}{Dt}(\Gamma_{CH_4}) - \nabla \cdot \left(\frac{\rho D_T}{L_{CH_4}} \nabla \Gamma_{CH_4} \right) = -\omega_I , \quad (16)$$

$$\rho \frac{D}{Dt}(\Gamma_{CO}) - \nabla \cdot \left(\frac{\rho D_T}{L_{CO}} \nabla \Gamma_{CO} \right) = \omega_I - \omega_{II} , \quad (17)$$

$$\rho \frac{D}{Dt}(\Gamma_{CO_2}) - \nabla \cdot \left(\frac{\rho D_T}{L_{CO_2}} \nabla \Gamma_{CO_2} \right) = \omega_{II} , \quad (18)$$

$$\rho \frac{D}{Dt}(\Gamma_{H_2O}) - \nabla \cdot \left(\frac{\rho D_T}{L_{H_2O}} \nabla \Gamma_{H_2O} \right) = 2\omega_I , \quad (19)$$

$$\rho \frac{D}{Dt}(\Gamma_{O_2}) - \nabla \cdot \left(\frac{\rho D_T}{L_{O_2}} \nabla \Gamma_{O_2} \right) = -\frac{3}{2}\omega_I - \frac{1}{2}\omega_{II} , \quad (20)$$

where use is made of the variable $\Gamma_i = Y_i/W_i = [i]/\rho$, with Y_i and W_i denoting the mass fraction and molecular weight for chemical species i, respectively, and ρ being the density. In the formulation, D/Dt is the substantial derivative and $D_T = \lambda/(\rho c_P)$ denotes the thermal diffusivity of the gas mixture, with λ and c_p representing its thermal conductivity and specific heat at constant pressure. A Fickian approximation is adopted here for the diffusion velocities, with $L_i = \lambda/(\rho c_p D_i)$ denoting the Lewis number of species i based on its diffusion coefficient D_i.

Similarly, the energy equation can be written for the thermal enthalpy $h_T = \int^T c_p \cdot dT$ as

$$\rho \frac{D}{Dt}(h_T) - \nabla \cdot (\rho D_T \nabla h_T) = q_I \omega_I + q_{II} \omega_{II} - 4\sigma T^4 l_p \quad (21)$$

where the overall heats of reaction are related to the enthalpies of formation per mole of species i, h_{fi}, by the equations $q_I = h^0_{CO} + 2h^0_{H_2O} - h^0_{CH_4}$, and $q_{II} = h^0_{CO_2} - h^0_{CO}$. In writing Eq. 21, a low Mach number approximation has been employed, and unsteady pressure variations have been neglected along with the effect of the differences of the specific heat at constant pressure of each species from the mean c_p. The radiative heat loss corresponds to that of an optically thin gas with cold boundaries, with σ denoting the Stephan-Boltzmann constant and l_p being the Plank mean absorption length, a function of the partial pressure of H_2O and CO_2 that varies according to $l_p \propto (\alpha_{CO_2}\Gamma_{CO_2} + \alpha_{H_2O}\Gamma_{H_2O})$, where the coefficients α_{CO_2} and α_{H_2O} are temperature dependent. To completely describe the reacting flow field, Eqs. 16-21 must be integrated together with the continuity and momentum equations with appropriate boundary and initial conditions.

5. ONE DIMENSIONAL FLAME

For a preliminary assessment of the model performance, we first consider the case of a one-dimensional nonradiating flame propagating at velocity u_u, a configuration for which numerical computations with detailed transport and chemistry can be easily performed. This study provides in particular expressions for calculating the parameters B and E. Explicit values for these two parameters are, however, not provided here.

5.1 Problem Formulation

For the following description, it is convenient to utilize a reference frame attached to the flame with x denoting the distance across the flame. In the formulation, the subscript u and b denote, respectively, properties in the unburnt ($x \to -\infty$) and burnt ($x \to \infty$) sides of the flame. With this notation, the steady one-dimensional form of the continuity equation reduces to $\rho u = \rho_u u_u$, while the x-component of the momentum equation is replaced by p=constant, thereby simplifying the problem to that of integrating Eqs. 16 - 21 with the transport operator written in the form:

$$\rho \frac{D(\,)}{Dt} - \nabla \cdot \left[\frac{\rho D_T}{L_i} \nabla(\,) \right] = \rho_u u_u \frac{d(\,)}{dx} - \frac{d}{dx}\left[\frac{\rho D_T}{L_i} \frac{d(\,)}{dx} \right] \quad (22)$$

The boundary conditions for the problem become:

a) $x=-\infty$

$$\Gamma_{CH_4} = \Gamma_{CH_4 u}$$
$$\Gamma_{CO} = \Gamma_{H_2O} = \Gamma_{CO_2} = 0$$
$$\Gamma_{O_2} = \Gamma_{O_2 u} ,$$
$$h_T = h_{Tu} ,$$

b) $x=\infty$

$$\frac{d\Gamma_{CH_4}}{dx} = \frac{d\Gamma_{CO}}{dx} = \frac{d\Gamma_{H_2O}}{dx} = \frac{d\Gamma_{CO_2}}{dx} = \frac{d\Gamma_{O_2}}{dx} = \frac{dh_T}{dx} = 0$$

Introducing the variables:

$$y_{CH_4} = \Gamma_{CH_4}/\Gamma_{CH_4 u} ,$$
$$y_{CO} = \Gamma_{CO}/\Gamma_{CH_4 u} ,$$
$$y_{H_2O} = \Gamma_{H_2O}/\Gamma_{CH_4 u} ,$$

$$y_{CO_2} = \Gamma_{CO_2}/\Gamma_{CH_4u},$$
$$y_{O_2} = (\Gamma_{O_2u} - \Gamma_{O_2})/\Gamma_{CH_4u},$$
$$\theta = (h_T - h_{Tu})/[(q_I + q_{II})\Gamma_{CH_4u}],$$

together with a new nondimensional coordinate $\eta = \int_0^x (u/D_T)dx'$, transform Eqs. 16-21 to

$$y'_{CH_4} - y''_{CH_4}/L_{CH_4} = -\varpi_I, \quad (23)$$
$$y'_{CO} - y''_{CO}/L_{CO} = \varpi_I - \varpi_{II}, \quad (24)$$
$$y'_{CO_2} - y''_{CO_2}/L_{CO_2} = \varpi_{II}, \quad (25)$$
$$y'_{H_2O} - y''_{H_2O}/L_{H_2O} = 2\varpi_{II}, \quad (26)$$
$$y'_{O_2} - y''_{O_2}/L_{O_2} = \frac{3}{2}\varpi_I + \frac{1}{2}\varpi_{II}, \quad (27)$$
$$\theta' - \theta'' = q_I\varpi_I + q_{II}\varpi_{II}, \quad (28)$$

where the prime denotes derivatives with respect to η. Also, the rates of fuel consumption and CO oxidation previously given in Eqs. 5 and 6 are scaled with $(\rho_u^2 u_u^2 \Gamma_{CH_4})/(\rho D_T)$ to give the dimensionless rates ϖ_I and ϖ_{II}, and $\bar{q}_I = q_I/(q_I + q_{II}) = 0.6473$ and $\bar{q}_{II} = q_{II}/(q_I + q_{II}) = 0.3527$ represent the fractions of heat released through fuel consumption and CO oxidation. Equations 23-28 must be integrated with boundary conditions $y_{CH_4} - 1 = y_{H_2O} = y_{CO} = y_{CO_2} = y_{O_2} = \theta = 0$ at $\eta = -\infty$ and $y'_{CH_4} = y'_{H_2O} = y'_{CO} = y'_{C_2O} = y'_{O_2} = \theta' = 0$ at $\eta = +\infty$.

Further simplifications follow from assuming that the Lewis numbers appearing in Eqs. 23–27 are unity, enabling the integration of linear combinations Eqs. 25–28 with Eqs. 23 and 24 to give

$$y_{CO_2} + y_{CO} + y_{CH_4} = 1, \quad (29)$$
$$y_{H_2O} + 2y_{CH_4} = 2, \quad (30)$$
$$y_{O_2} + \frac{1}{2}y_{CO} + 2y_{CH_4} = 2, \quad (31)$$

and

$$\theta + \bar{q}_{II}y_{CO} - y_{CH_4} = 1, \quad (32)$$

as replacements for Eqs 25-28 in the following development.

5.2 The CO-oxidation region

As previously explained, reaction I is much faster than reaction II, and therefore takes place in a layer that is much thinner than the CO-oxidation region. Because of this relative scaling, for the analysis of this CO-oxidation region one can replace ϖ_I by a dirac-delta function located at the fuel consumption sheet. Also, due the translational invariance of the one dimensional problem, one can choose $\eta = 0$ as the location for the fuel-consumption sheet, thereby reducing the problem to that of integrating

$$y'_{CH_4} - y''_{CH_4} = -\delta(\eta) \quad (33)$$

and

$$y'_{CO} - y''_{CO} = \delta(\eta) - \varpi_{II} \quad (34)$$

supplemented by Eqs. 29-32. On the other hand, since the solution to Eq. 33 is simply $y_{CH_4} = 1 - \exp(\eta)$ for $\eta < 0$ and $y_{CH_4} = 0$ for $\eta > 0$, the problem further simplifies to that of integrating

$$y'_{CO} - y''_{CO} = -\varpi_{II} \quad (35)$$

with boundary conditions $y_{CO} - y'_{CO} = 1$ at $\eta = 0$ and $y'_{CO} = 0$ as $\eta \to \infty$. The dimensionless rate of CO oxidation is calculated from

$$\varpi_{II} = \left(\frac{\rho^2}{\rho_u^2}\right)\left(\frac{\rho\Gamma_{CH_4u}k_{4f}}{u_u^2/D_T}\right)\left(y_{CO} - \frac{K_5}{K_4}\frac{y_{CO_2}y_{H_2}}{y_{H_2O}}\right)y_{OH} \quad (36)$$

To integrate Eq. 35, use must be made of expressions $y_{CO_2} = 1 - y_{CO}$, $y_{H_2O} = 2$, $y_{O_2} = 2 - y_{CO}/2$ and $\theta = 1 - q_{II}y_{CO}$, which follow from Eqs. 29-32 with $y_{CH_4} = 0$, and also of Eqs. 7 and 8 for the computation of the steady-state values of the variables $y_{OH} = \Gamma_{OH}/\Gamma_{CH_4u}$ and $y_{H_2} = \Gamma_{H_2}/\Gamma_{CH_4u}$.

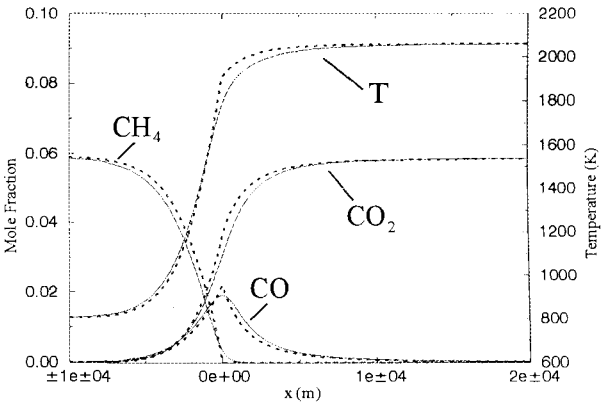

Figure 2: The variation of the temperature and of the CH_4, CO and CO_2 mole fractions across the unstretched one-dimensional flame corresponding to test-case A., as obtained with detailed chemistry (solid lines), and with the two-step model with infinitely fast fuel consumption (dotted lines).

Integration of the autonomous Eq. 35 with the aforementioned boundary conditions can be easily performed with a simple shooting method. For simplicity in the calculations, constant values of $c_p = (c_p)_b$ and $\rho^2 D_T = (\rho^2 D_T)_b$ were assumed, and the variations of the density with composition were neglected, so that $\rho = \rho_b T_b/T$. The results for the simple model were compared with those of numerical integrations of the full conservation equations with detailed transport and chemistry (see [4] for a description of the chemical-kinetic mechanism employed). The "FlameMaster" code [5] previously used for instance in [6], is utilized in the detailed calculations. Conditions of test cases A and B were selected for the comparisons, namely, T_u = 800 K, p = 18 bar and ϕ = 0.6, and T_u = 900 K, p = 40 bar and ϕ = 0.6. In integrating Eq. 35 the function ϖ_{II} was evaluated with the value of u_u extracted from the detailed chemistry calculations.

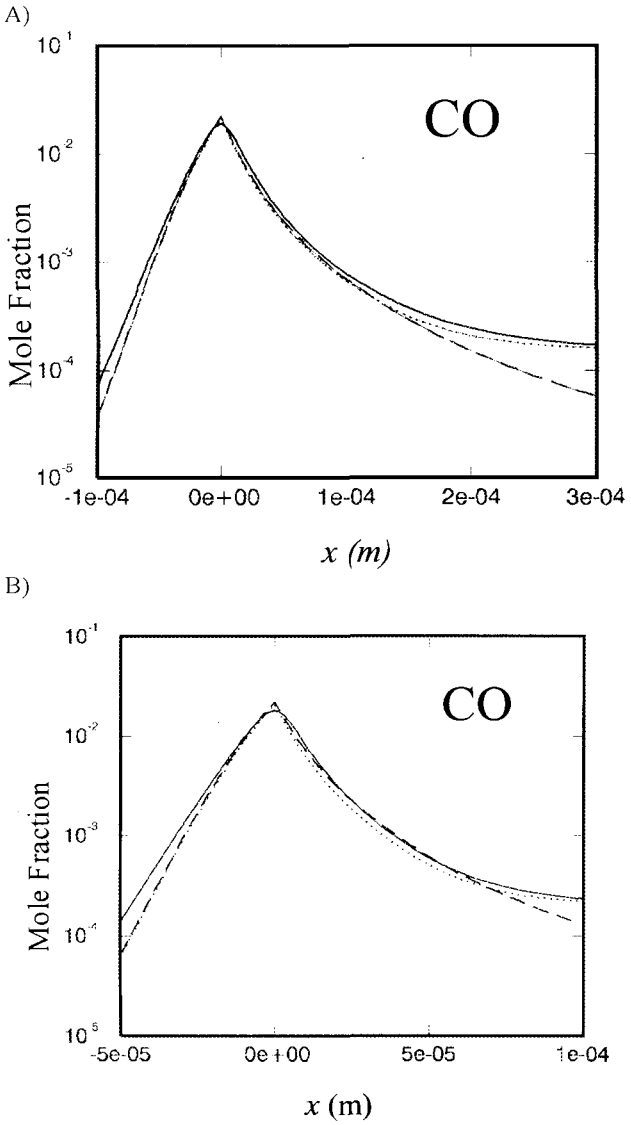

Figure 3: The variation of the CO mole fraction across the unstretched one-dimensional flame as obtained with detailed chemistry (solid lines), with the complete two-step model (dotted lines) and with two-step model with HO_2 recombination neglected (dashed lines). A) Test case A. B) Test case B.

The characteristic flame structure corresponding to the reduced two-step model is shown in Figure 2, along with the results of detailed chemistry calculations. Because of the infinitely fast fuel-consumption rate incorporated, the results of the two-step model exhibit an infinitely thin fuel-consumption layer across which the profiles of temperature, CH_4 and CO present discontinuities in derivatives, while the CO_2 whose rate of production is independent of ϖ_1, remains smooth. In the detailed calculations, however, the thin fuel-consumption layer remains of finite thickness. For the mutual comparison of the results of the two approaches, the point were the CO profile reaches its peak value is selected here as a suitable definition for the location of the fuel-consumption layer of the detailed calculations. Adoption of a different definition, e.g., point where the CH_4 concentration falls below an appropriate small threshold value, would result in a small relative translation of the different profiles by an amount of the order of the fuel-consumption layer thickness.

As can be seen, the two-step model adequately reproduces the shape and the peak value of the profile of CO mole fraction, with significant departures appearing only inside the fuel-consumption layer, where the detailed-chemistry profiles are rounded because of finite rate effects. To further illustrate this agreement, profiles of CO corresponding to the two sets of conditions previously mentioned are plotted in logarithmic scale in Figure 3. The resulting plots clearly show how the proposed formulation remains accurate as equilibrium is approached downstream from the flame, with the minimal departures in the final CO equilibrium values seen in Figure 3 being related to the truncated steady-state expression 4 utilized in the computations.

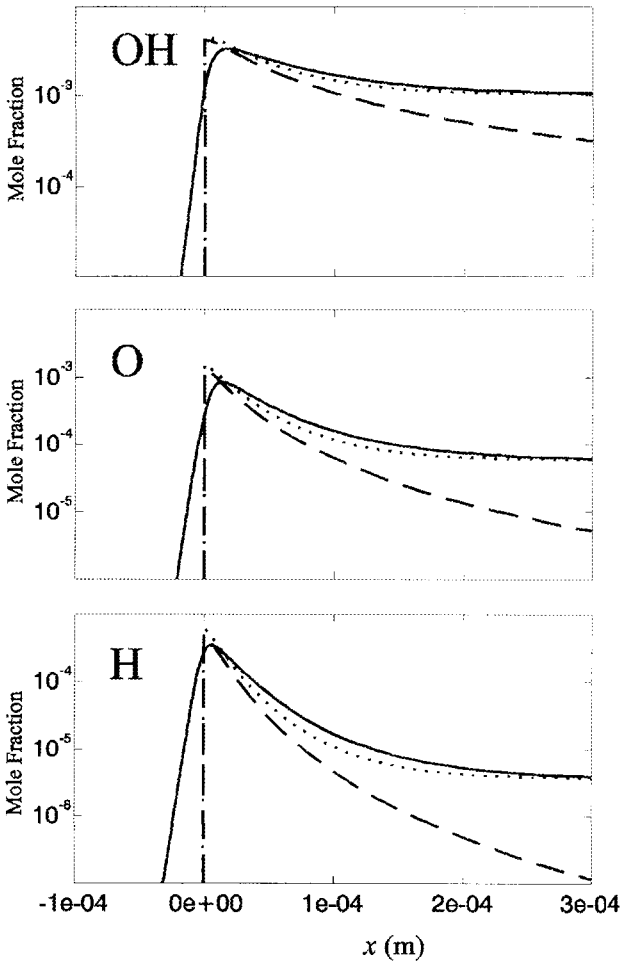

Figure 4: The variation of radical mole fractions across the unstretched one-dimensional flame as obtained with detailed chemistry (solid lines), with the complete two-step model (dotted lines) and with two-step model with HO_2 recombination neglected (dashed lines). Test case A.

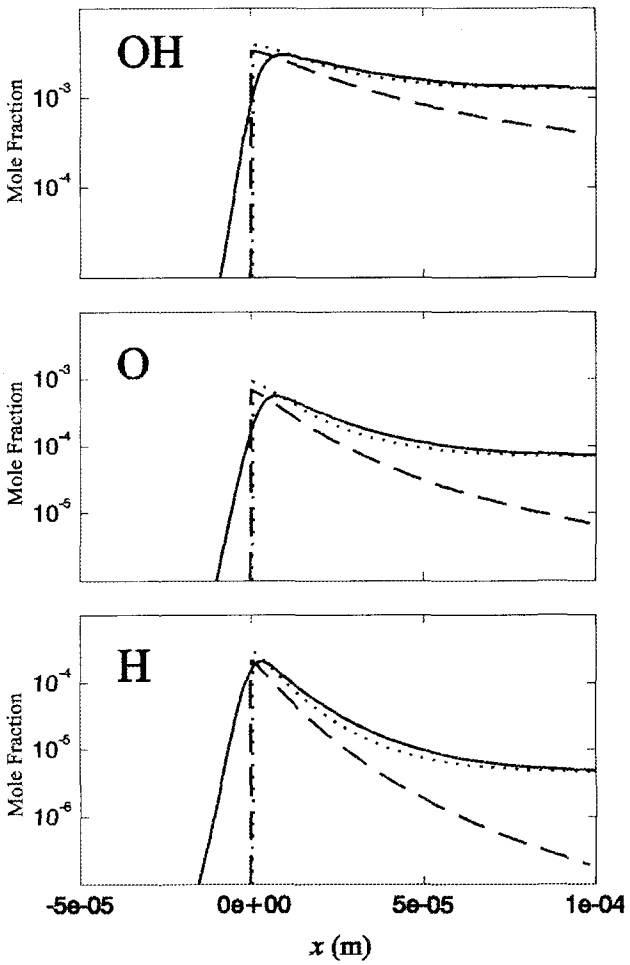

Figure 4 (cont.): The variation of radical mole fractions across the unstretched one-dimensional flame as obtained with detailed chemistry (solid lines), with the complete two-step model (dotted lines) and with two-step model with HO_2 recombination neglected (dashed lines). Test case B.

The proposed model also succeeds in predicting OH, O and H profiles across the flame, as can be seen in Figure 4, where radical mole fractions obtained from Eqs. 2, 3 and 8 are compared with results of detailed computations. The two-step model adequately describes both, the peak concentration and the profile evolution towards equilibrium. Because of fast radical depletion through fuel consumption, the radical concentrations of the detailed chemistry computations show very steep gradients upstream from the fuel consumption layer, rapidly approaching the zero value corresponding to the two-step model. It can also be seen that the radical profiles obtained with detailed chemistry peak slightly downstream from the location of maximum CO concentration, a characteristic not seen in the results of the two-step model that follows from the inner structure of the fuel-consumption layer [2].

5.3 The Limit of Irreversible Radical Recombination

Neglecting the reverse of the radical-recombination reaction III', a simplification adopted in previous asymptotic analyses [2, 3], leads to the reduced CO-oxidation rate previously given in Eq. 15. Since use of this more compact expression would somewhat reduce the effort required in computations, it is of interest to test the accuracy of the resulting approach. Introducing Eq. 15 into Eq. 36 reduces the problem to that of integrating

$$y'_{CO} - y''_{CO} = -\Delta y_{CO}^{3/2} \tag{37}$$

with boundary conditions $y_{CO} - y'_{CO} = 1$ at $\eta = 0$ and $y'_{CO} = 0$ as $\eta \to -\infty$. The Damköhler number

$$\Delta = \left(\frac{k_{4f}}{k_{3f}[M]} \frac{K_2 (1-\gamma)\alpha_2^3}{K_6} \right)^{1/2} \left(\frac{\rho^2}{\rho_u^2} \right) \left(\frac{\rho \Gamma_{CH_4 u} k_{4f}}{u_u^2 / D_T} \right) \tag{38}$$

is a function of the temperature and, more weakly, of the mixture composition (through the function α_2) that usually takes fairly large values in the CO-oxidation region. For instance, evaluation of Eq. 38 at the equilibrium condition corresponding to the two test cases previously defined gives $\Delta = 9.36$ for $T_u = 800$ and $\Delta = 10.45$ for $T_u = 900$.

Results of integration of Eq. 37 with the aforementioned boundary conditions are included in Figures 3 and 4. As can be seen in the calculations, the reduced model adequately describes the CO profiles, including the peak values and the initial decrease due to CO oxidation. However, with irreversible radical recombination, the resulting description fails to reproduce the final equilibrium value, approaching instead a zero CO concentration far downstream from the flame. A similar behavior is found for the radical profiles, with significant departures appearing at somewhat smaller distances downstream. Since a detailed knowledge of the radical pool everywhere across the flame is fundamental to calculate NO emissions, the results in Figure 4 suggest that the complete model, including Eqs. 7 and 8 for calculating the concentrations of H_2 and OH, should be considered for increased accuracy in computations.

Despite the limitations exhibited, the reduced CO-oxidation ratio given in Eq. 15 describes the CO profile over about two orders of magnitude in CO mole fraction. To further investigate the resulting solution, use can be made of relatively large value of parameter Δ by considering the solution to Eq. 37 for $\Delta >> 1$, an asymptotic limit also utilized in previous studies [3]. Since in this limiting case CO oxidation occurs in a region of thickness much smaller than that of the flame, we can neglect in the first approximation variations of Δ. The resulting solution is determined at leading order by a balance between diffusion and reaction as can be exposed by introducing the stretched variable $Y = \Delta^{2/5} y_{CO}$ and the associated stretched coordinate $\zeta = \Delta^{2/5} \eta$, thereby transforming the problem to that of integrating $\ddot{Y} - \Delta^{-2/5} \dot{Y} - Y^{3/2}$, with boundary conditions $\dot{Y} - \Delta^{-2/5} Y = -1$ at $\zeta = 0$ and $Y = 0$ as $\zeta \to \infty$. Here, the dot denotes derivatives with respect to the coordinate ζ. Introducing the asymptotic expansions $Y = Y_0 + \Delta^{-2/5} Y_1 + \ldots$ in the above equation and boundary conditions, and collecting terms in powers of Δ yields leading-order problem $\ddot{Y}_0 = Y_0^{3/2}$, $\dot{Y}_0(0) = -1$ and $\dot{Y}_0(\infty) = 0$, which can be readily integrated to give

$$Y_0 = \left(\frac{5}{4} \right)^{5/2} \left[1 + \frac{1}{4} \left(\frac{4}{5} \right)^{2/5} \zeta \right]^{-4} \tag{39}$$

Equation 39 determines the peak value of $y_{CO} = (5/4)^{5/2}\Delta^{-2/5}$ and also reveals a fast decay of the CO concentration according to $Y_0 \propto \zeta^{-4}$ as $\zeta \to \infty$. Because of the reaction-rate dependence on $y_{CO}^{3/2}$ appearing in Eq.37 [7], the decaying rate changes downstream as the effect of convection becomes nonnegligible, which occurs at distances η of order unity ($\zeta \approx 0[\Delta^{2/5}]$) when the CO concentration y_{CO} reaches small values of order Δ^{-2} ($Y \approx 0[\Delta^{-5/8}]$), ushering in a convective-diffusive-reactive region whose structure is described in terms of the variable $y = \Delta^2 y_{CO}$ by integrating

$$y'' - y' = y^{3/2} \tag{40}$$

with leading-order boundary conditions $y \to \infty$ at $\eta=0$ and $y' \to 0$ as $\eta \to \infty$. The solution to this parameter–free problem, which is exhibited in Figure 5 for completeness, describes the evolution of the rate of decay of the CO mole fraction across this convective-diffusive-reactive region from the initial rate $y \propto \eta^{-4}$ of the diffusive-reactive region, to the slower rate $y \propto \eta^{-2}$ corresponding to the final convective-reactive balance that appears at distances $\eta >> 1$. Clearly, this simplified analysis of irreversible radical recombination ceases being valid as the CO mole fraction emerging from Eq. 37 decreases to a value comparable to that of chemical equilibrium.

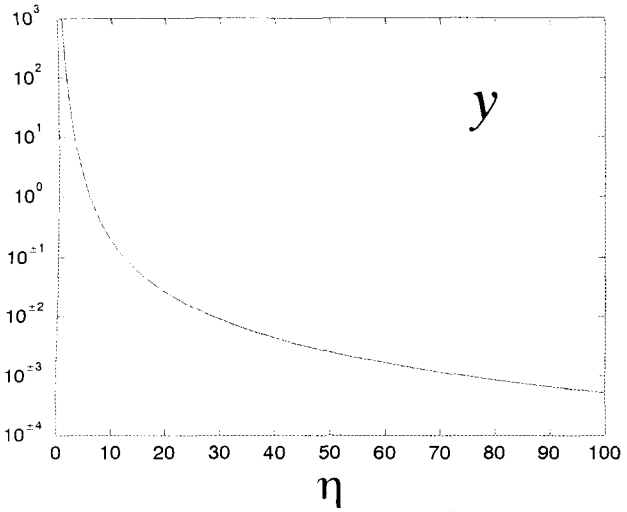

Figure 5: The variation of the function $y=\Delta^{-2}y_{CO}$ as obtained from integration of Eq. 40.

5.4 The Fuel-Consumption Layer

The previous asymptotic analysis $\Delta>>1$ yields in the first approximation $(y_{co})_f = (5/4)^{5/2}\Delta^{-2/5}$ and $(y'_{CO})_f = -1$ as the peak value and slope of the CO concentration profile at the fuel-consumption layer, where the temperature , T_f, is given in the first approximation by

$$\theta_f = \frac{T_f - T_u}{T_b - T_u} = 1 - (5/4)^{(5/2)}\bar{q}_{II}\Delta^{-2/5} \tag{41}$$

as follows from Eq. 32 with

$$T_b - T_u = \frac{(q_I + q_{II})\Gamma_{CH_4,u}}{c_p} \tag{42}$$

These simplified results are useful in describing the inner structure of the fuel-consumption layer, which is studied below by activation energy asymptotics.

Owing to its small thickness, convection and CO-oxidation are negligible in the fuel-consumption layer, thereby enabling integration of a linear combination of Eqs. 23 and 28 to give

$$\theta - \theta_f = \frac{T - T_f}{T_b - T_u} = \bar{q}_I\left(\gamma\eta - y_{CH_4}\right) \tag{43}$$

where $\gamma = q_{II} / q_I = 0.5448$. Assuming that the modified Zeldovich number

$$\beta = \frac{E(T_b - T_u)\bar{q}_I}{R^o T_f^2} \tag{44}$$

is an asymptotically large quantity and introducing the rescaled variables $\phi = \beta y_{CH_4}$, and $\xi = \beta\eta$, reduces Eq. 23 to

$$\frac{d^2\phi}{d\xi^2} = \frac{1}{2}\lambda\phi\exp(-\phi + \gamma\eta) \tag{45}$$

to be integrated with boundary conditions $\phi(-\infty) = -\xi$ and $\phi(\infty) = 0$. This canonical problem was previously encountered by Liñán [8] when studying the inner structure of diffusion flames in the premixed flame regime. In particular, he computed the value of the reduced Damköhler number

$$\lambda = 2\frac{\rho^2 D_T}{\rho_u^2 u_u^2}\frac{B}{\beta^2}\exp\left[-E/(R^o T_f)\right] \tag{46}$$

as a function of the heat-loss parameter γ, obtaining $\lambda \approx 1.9$ for the particular value $\gamma = 0.5448$ of interest here. Incorporating this result enables the calculation of the flame velocity u_u from Eqs. 38, 41, 42, 44 and 46.

6. CONCLUSIONS

The main contribution of the present study is the development of a two-step reduced mechanism adecuate for computation of premixed reacting flows under LPP combustion conditions. The analysis incorporates a fast fuel consumption step that produces CO, and a much slower CO-oxidation step. Results corresponding to one-dimensional flames indicate that the model describes satisfactorily the flame structure including profiles of all relevant intermediates and temperature. Furthermore, an Arrhenius rate with large activation energy is proposed here for the fuel consumption step. Equations relating the preexponential factor and the activation energy of the presumed rate with the laminar flame velocity, mixture composition, pressure, and upstream temperature are obtained through a rigorous asymptotic analysis of the resulting fuel consumption layer, thereby facilitating the selection of the reaction-rate parameters. Closure of the proposed two-step model through this selection and further testing are currently being performed.

7. ACKNOWLEDGEMENTS

This investigation was mainly supported by the European LOWNOX-III research project, contract BRPR-CT-95-0122, included in the EU sponsored Brite-Euram Aeronautics

program. Additional funding was obtained through the Spanish National Research and Technology Program, under grant CICYT-C95013002.

8. REFERENCES

[1] Baulch, D., Cobos, C., Cox, R., Frank, P., Hayman, G., Just, Th., Kerr, J., Murrels, T., Pilling, M., Troe, J., Walker, R., Warnatz, J. Combust. Flame **98**, p. 59 (1994)

[2] Peters, N. and Williams, F. A., Combust. Flame **68**, p.185 (1987).

[3] Bui-Pham, M., Seshadri, K., and Williams, F. A., Combust. Flame **89**, p. 343 (1992).

[4] Peters, N., in Reduced Kinetic Mechanisms for Applications in Combustion Systems (N. Peters, and B. Rogg, Eds.) Lecture Notes in Physics m15, Springer-Verlag, 1993, p. 3.

[5] Pitsch, H., and Bolling, M.: "FlameMaster, A Computer Code for Homogeneous and One-Dimensional Laminar Flames Calculations". Institut für Technische Mechanik, RWTH-Aachen (1994).

[6] Hewson, J., and Bolling, M., Twenty-Sixth Symposium (International) on Combustion, The Combustion Institute, Pittsburgh, PA, 1996, p. 2171.

[7] Williams, F. A., Combustion Theory. Benjamin Cummings, Menlo Park, CA, 2nd editions, 1985, p. 162.

[8] Liñán, A., Acta Astronautica **1**, p. 1007 (1974).

PAPER No. 12
Bollig, Linan, Lazaro & Sanchez
(presenter: A. Sanchez)

Question 1: M. Pourkashanian, University of Leeds, U.K.

Reduced reaction mechanisms like this should only be used for situations where they are validated. They tend to fail for diffusion flames. Was the mechanism reduced by examining the local Jacobians?

Answer:

We would agree with the comments. For reduction of the mechanism we did not examine the Jacobians, but rather used fluxes and sensitivities with respect to the flame velocities calculated.

Question 2: S. Wittig, University Karlsruhe, Germany

Did you analyze the predictions of Zeldovich NOx made for the reduced mechanism? It appears as though the radical pool is not adequate and the concentrations not accurate enough to get nitric oxide correct.

Answer:

Yes, we did try, and you are right, the radical pool is inadequate so we over-predicted NO by 20%. However, the rates of both nitrous oxide production and the thermal mechanisms of NO prediction depend linearly on the O-atom concentration. Therefore, the departures found are not very significant, and are limited to the rate of NO production in the thin, fuel-consumption layer.